Transactions, SMiRT-23
Manchester, United Kingdom - August 10-14, 2015
Division I, Paper ID 194

SELF-CONSOLIDATING ULTRA-HIGH PERFORMANCE CONCRETE FOR SMALL MODULAR REACTOR CONSTRUCTION

Mo Li[1], Ing Lim[1], Jamshaid Sawab[1], and Y.L Mo[1]

[1] Department of Civil and Environmental Engineering, University of Houston, Houston, Texas, USA

ABSTRACT

Small modular reactors (SMR) allow for faster onsite construction, increase nuclear material security, and provide a flexible and cost-effective power source. SMR can be factory-built as modular components, and shipped to desired locations for fast assembly. This study developed a new type of ultra-high performance concrete (UHPC) which features a compressive strength higher than 150 MPa and self-consolidating characteristics desired for SMR modular construction. With a high strength and dense microstructure, it will facilitate rapid construction of steel plate-concrete (SC) beams and walls with thinner and lighter modules, and can withstand the harsh environments and mechanical loads anticipated during the service life of nuclear power plants. The self-consolidating characteristics are crucial for fast construction and assembly of SC modules with reduced labor costs and improved quality. This paper describes the development and characterization of self-consolidating UHPC, its large-scale processing techniques with conventional equipment, and the ongoing work on the structural mechanics of SC modules made of self-consolidating UHPC.

INTRODUCTION

Steel plate-concrete (SC) is used to build shields in AP1000 nuclear power plants. SC is a composite structure system consisting of two layers of steel plates and a sandwiched concrete layer in between. Cross ties are used to increase the shear carrying capacity of SC modules by enhancing efficiency of shear transfer between the steel plates and concrete (Subedi, 2003; Xie et al., 2007). SC modules have good potential for small modular reactors (SMR) because of their cost-effectiveness and reduced construction time. This paper presents a new type of ultra-high performance concrete (UHPC) to replace conventional concrete in SC modules for SMR. The UHPC can improve SMR design by using less concrete and steel, taking advantage of the high strength and durability of UHPC. As a result, SMR design and construction with optimized efficiency, compactness and reduced costs can be achieved. The modularity and ease of assembly of steel plate-UHPC (S-UHPC) beams and walls addresses the high cost barriers of typical nuclear power plants, and can provide large benefits to the electric power industry.

Research on high strength concrete or high performance concrete (HPC) with compressive strength higher than 100 MPa has been carried out over the past decades. However, their direct application in nuclear power plant construction does not yet exist. Attaining compressive strengths over 150 MPa without special treatment such as high pressure curing, heat curing and extensive vibration, has remained a challenge. Also, lack of standardized processing and quality control methods to produce robust HPC materials in large quantities has limited its application in factory prefabrication. At the structural scale, when a SC beam is subjected to both flexure and out-of-plane shear, cross ties within the concrete connecting the two steel faceplates need to be designed to ensure the integrity of the SC module. When HPC is used in SC structures, large-scale experiments need to be conducted to understand the structural behavior and determine the minimum amount of cross ties.

This paper presents the development of self-consolidating UHPC that can be produced in mass quantities. The material development approach integrates micromechanics theory, hydration chemistry, rheology

tailoring methods, and time-dependent computed micro-tomography (Micro-CT) that can characterize material 3D microstructure formation and degradation. The new UHPC possesses a compressive strength exceeding 150 MPa without special heat and pressure treatment, by using a conventional concrete mixer and ingredients commercially available in the U.S. To bridge the gap between laboratory development and construction application, quality control methods were developed to ensure robust production of UHPC modules in mass quantities. S-UHPC beams were manufactured at large-scale to test their structural performance under flexure and shear. Based on these results, new design guidelines for S-UHPC modules can be developed for SMR applications.

EXPERIMENTAL PROGRAM

Materials

The UHPC developed in this study contains cement, fine sand, ground quartz, silica fume, silica powder, high-range water reducer (HRWR) and water. Low water to cement ratio is required to achieve high compressive strength, as well as fine grains for high packing density. Two types of cement were investigated: Type I Portland cement that is an ordinary, general purpose cement, meets ASTM C150 specification and meets the low alkali requirements; and Class-H cement that is an oil well cement with zero calcium aluminate (C_3A) content and has coarser particle size compared to Type I ordinary Portland cement. The low C_3A content leads to slower hydration, longer setting time and higher flowability. Coarser particles reduce the water requirement in the mixture while maintaining the same flowability.

Mineral admixtures silica fume and fly ash were used. Silica fume was found to be the most effective means of manufacturing very high strength concrete. In the form of ultra-fine particles, silica fume functions as micro-fillers, and its pozzolanic reaction improves the packing density of the matrix. It also prevents segregation caused by the use of large quantities of HRWR. Previous studies have recommended the optimum proportion of silica fume to be 20-25% by weight of cement (Larrard, 1992). Three different types of silica fume (SF), i.e. regular densified silica fume (DSF), undensified silica fume (USF) and white silica fume (WSF), were used to study their effect on the UHPC mixture (Figure 1). Low calcium Class F fly ash was added to the mixture to increase the flowability due to its spherical shape.

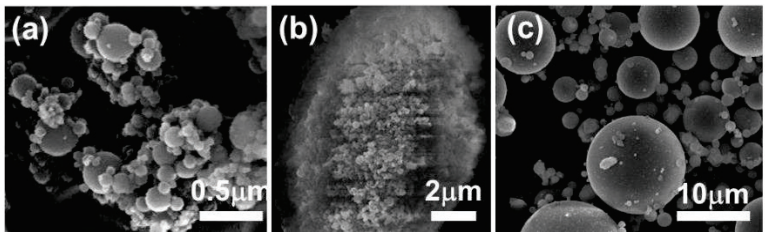

Figure 1 SEM images of (a) grain particles of USF (b) one grain of DSF (c) fly ash particles

The solid particles also include round quartz crystalline silica that is chemically inert with >99.7% silicon dioxide content. Unground silica passing the sieve size of 850 micron is used as coarse sand, and ground silica (GS) passing the sieve size of 212 micron is used as fine sand. Fine ground silica (FGS) in the form of white powder is used as micro-filler for better packing density. Median diameter of the fine ground silica is 1.6 micron, and 96% of the powder has a diameter smaller than 5 micron.

High-range water reducer is used to achieve good workability with a very low water-cement ratio for self-consolidating UHPC. Three different types of Polycarboxylate-based HRWR that are commercially available in the U.S. were investigated, with different amounts of dosage.

Particle Size Distribution

Size distributions of the constituent materials characterize the packing density in a mixture. Figure 2 shows the particle size distribution of aggregates, cementitious and pozzolanic ingredients of UHPC mixture. The particle size distribution analysis was performed using two equations (Brouwers and Radix, 2005; Funk and Dinger, 1928; Yu et al., 2014): one suggested by Andreasen and Andersen (Equation 1), and another by Funk and Dinger (Equation 2).

$$P = \left(\frac{d}{D} \right)^{q} \times 100 \tag{1}$$

$$P = \left(\frac{d^{q} - dm^{q}}{D^{q} - dm^{q}} \right) \times 100 \tag{2}$$

Where P is the cumulative passing percentage, d is the corresponding sieve size, D is the diameter of the largest particle, dm is the minimum particle size in the distribution, and q is the coefficient of distribution that is a selected parameter between 0 and 1. Andreasen and Andersen [4-6] found that optimum packing is obtained when q = 0.37, which is the maximum limit to achieve zero voids condition based on computer simulation. Distribution modulus q determines the slope of the particle distribution curve in both equations. A mixture with more coarse particles better fits the curve with higher distribution modulus, and a mixture with more fine particles better fits the curve with lower distribution modulus (Elkem, 2014; Funk and Dinger, 1928). Comparison between distribution curves with different q values is shown in Figure 2 (c).

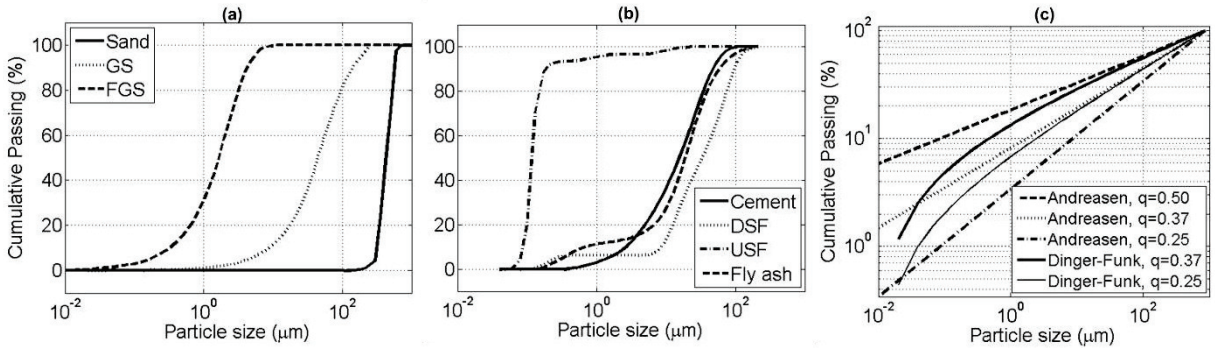

Figure 2 (a) and (b) Particle distribution of aggregates, cementitious and pozzolanic ingredients
(c) Comparison between different models of particle size distribution curves

Specimen Preparation and Test Setup

The compressive cylinder specimens were prepared using a 4.7 L capacity force-based mixer. Flowability was tested using a flow cone conforming to ASTM C230. The specimens were demolded 48 hours after casting and were cured in water until 28 days for compressive testing with displacement control at a rate of 0.5 mm/min.

Large-scale mixing was conducted using a 0.3 m^3 capacity gravity-based mixer. In order to evaluate the self-consolidating properties of UHPC processed at large scale, slump-flow, J-ring, and V-funnel tests were conducted (Figure 3). Slump flow test was done to measure the flowability and filling ability according to ASTM 1611, with the upright mold procedure by Abram's cone that conforms to ASTM C143. Segregation resistance was measured by V-funnel test at 5 minutes after filling as well as through a visual stability index (VSI, ASTM C1611 Appendix). J-ring test was done to measure the passing ability of UHPC, according the ASTM C1621. The air content at fresh state for both mixtures was also measured according to ASTM C231 with a type-B air meter.

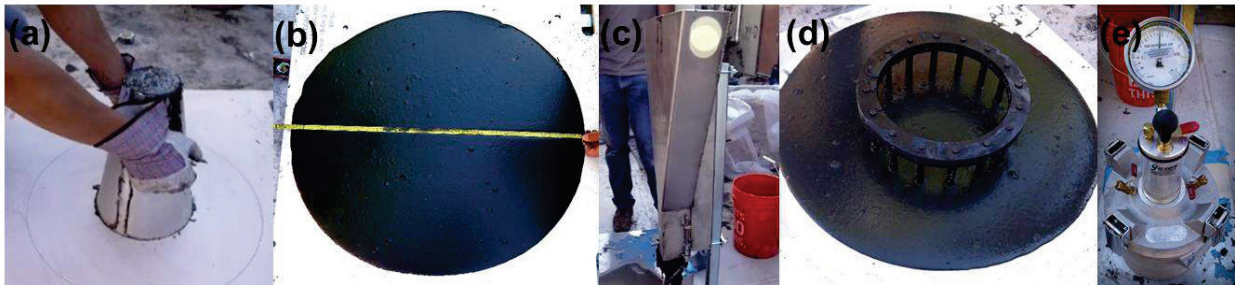

Figure 3 (a) Upright mold Abram's cone, (b) Slump flow measurement, (c) V-funnel test, (d) Passing ability test with J-ring (e) Air content measurement

Three-dimensional micro-computed tomography (μCT) was conducted to quantify the internal microstructure of various UHPC designs, in comparison with conventional concrete. Scanning Electron Microscopy was also adopted to analyze the surface microstructure topography of UHPC. These results were essential for understanding the impact of different mix designs on the formed hydration products and UHPC microstructure, and their consequent indication on UHPC composite mechanical properties and durability. The details of these studies will be reported in a journal paper.

S-UHPC Beams with Cross Ties

Two S-UHPC beams were tested to identify the minimum shear reinforcement ratio ($\rho_{t,min}$) for ductile shear behavior. SC beam design of a typical nuclear containment structure was adopted in this study and scaled down by a factor of 4/9. The length, width and depth of the SC beam were calculated to be 4.57 m, 0.3 m, and 0.4 m (Varma et al., 2011). This study used cross ties ratio ($\rho_{t,\,test}$) as the main parameter. Two different $\rho_{t,\,test}$ were used in each beam, resulting in four different cross ties ratio that began at 0.184% at S-UHPC-1 South (minimum shear reinforcement ratio recommended in ACI 318 for reinforced concrete beams) and was further increased by 25% (S-UHPC-1 North), 50% (S-UHPC-2 South) and 75% (S-UHPC-2 North) respectively of S-UHPC beams. Shear span (a) was defined as the distance between the loading point and the center line of the support (Figure 4). Previous research reported that the shear at failure depends on the shear span to depth ratio (a/d), and the minimum load carrying capacity occurs at a/d=2.5 (Ferguson and Clark, 1951; Kani, 1964; Qin et al., 2015). Therefore in this study, a/d was kept constant at 2.5 as the most critical loading condition for shear.

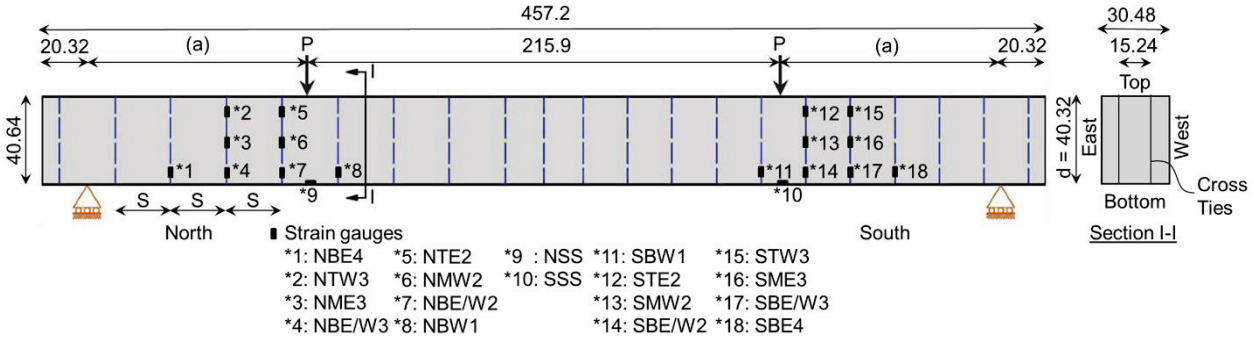

Figure 4 Elevation and strain gauge arrangement of S-UHPC beam

The diameter of the rebars and the spacing (S) of the cross ties were calculated based on the designed shear reinforcement ratio. No. 3 rebars were used as the shear reinforcement and grade 70 high strength steel conforming to ASTM/ASME SA 516 was used as the top and bottom steel plates. HBM Spider 8 DAS was used to continuously record the data from the load cells, LVDTs and strain gauges. In addition, the real-

time plots of strains in concrete, cross ties, and steel plates were used to observe and monitor the structural behavior of the specimen during the tests. Strain gauge labelling method is shown in Figure 5.

The beams were subjected to 2670 kN vertical loading at each actuator. The MTS Flex system was used to control the loads and displacements of the actuators. The displacement control feature was essential in capturing the post peak behavior of SC beams. Loading steps in the loading protocol were planned for a constant loading rate of 2.5 mm per 15 minutes. The cracks and the bond between the steel plates and UHPC were continuously monitored and recorded during the tests. Each end of the beams was tested individually.

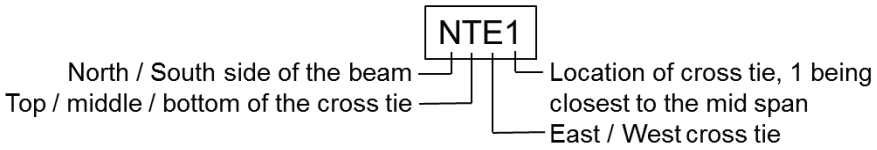

Figure 5 Labelling of the strain gauges

RESULTS AND DISCUSSION

Strength and Flowability

Various mixture proportions were tested to achieve the optimum flowability and compressive strength with different parameters such as the amount of fly ash, silica fume, FGS; and different types of superplasticizer, cement, and silica fume. To achieve the desired compressive strength, water to binder ratio was kept as low as 0.21, while maintaining an acceptable flowability. To limit the varying parameters, the ratio between silica fume and FGS was fixed at 1:1. Their content to cement ratio by weight from 0-0.25 was investigated. Figure 6 (a) and (b) show that 0.2 silica fume and FGS content led to the most optimum spread value (26 cm) and achieved the desired compressive strength. This series of mixtures used Portland cement type-I, USF, and 5% FA/C.

The amount of fly ash between 0 to 20% to cement by weight was investigated. It was found that 5% fly ash was most effective in significantly increasing flowability without sacrificing the 28 days compressive strength (Figure 6 (c) and (d)). Type I Portland cement was used in both series, involving two different types and amounts of silica fume (i.e. 0.25 DSF/C and 0.2 USF/C). It was found that different types of silica fume resulted in significant difference for flowability, but not for compressive strength.

Another parameter investigated was the type and amount of high range water reducer (HRWR) (Figure 6). Three types of superplasticizer were tested using 0.25 DSF and FGS to cement ratio, resulting in spread values of 16 cm, 11.5 cm and 17.5 cm respectively. Based on the compressive strength shown in Figure 7 (a), HRWR type C was selected for use in large scale testing.

Different types of silica fume also led to modified flowability. High shear energy was required to reverse the agglomeration of nanoparticles in DSF, thus most particles did not behave as spherical filler at fresh state. Weak bonds between particles in USF made it easy to break them apart during mixing, resulting in better flowability. Figure 7 (b) and Table 1 show that compared with the mixture of Portland cement type I and DSF, USF resulted in higher flowability and compressive strength. In most cases, a more workable mixture contained less air voids in the mixture, leading to higher compressive strength. Incorporating Class H cement in the mixture further improved flowability; however it also led to reduced strength due to the low C_3S content in Class H cement.

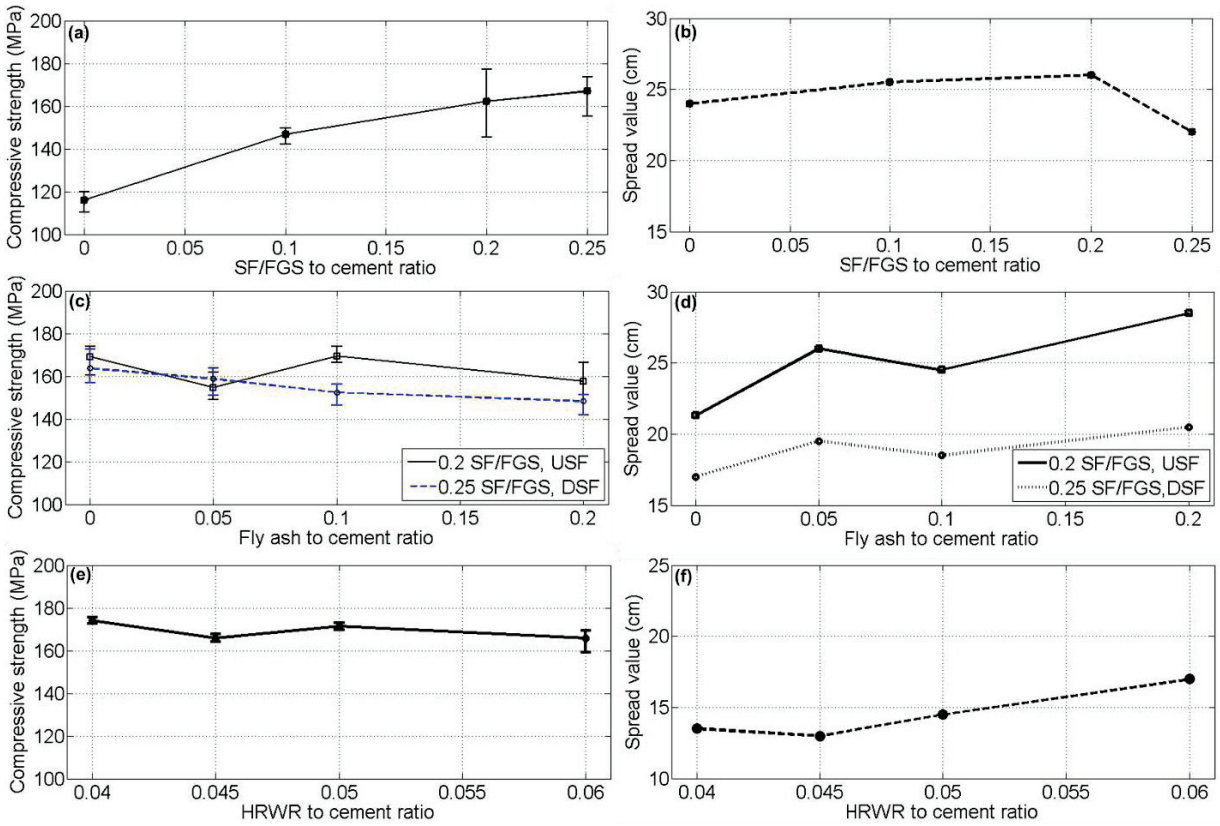

Figure 6 The effect of (a, b) silica fume and FGS content, (c, d) fly ash content, (e, f) amount of superplasticizer on compressive strength and spread value

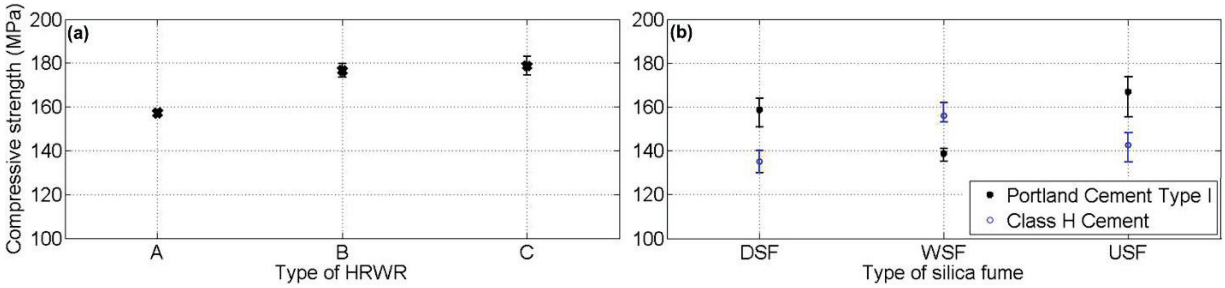

Figure 7 Effect of different type of HRWR and silica fume on compressive strength

Table 1: Effect of the type of silica fume on the flowability of mixtures with two different types of cement

Spread value (cm)	DSF	WSF	USF
Portland cement type I	19.5	18.0	22.0
Class-H cement	21.5	24.5	25.0

Particle Size Distribution and Self-Consolidating Properties

Particle size distributions of mixtures with 25% silica fume (USF compared with DSF), 25% FGS and 0% or 5% fly ash are shown in Figure 8. These curves fit the Dinger-Funk model better for optimal packing density, with a lower standard deviation. However, both Andreasen and Dinger-Funk models have lower slope on USF mixture. Higher distribution modulus signifies coarser particles and thus less flowability.

Moreover, the comparison between the mixture (5% fly ash) containing DSF and the theoretical model resulted in a standard deviation value of 5.03, which is significantly higher than the mixture containing USF with a standard deviation value of 4.07. This explains the higher spread value of the mixture containing 0.25 USF (22 cm and 19 cm for 5% and 0% fly ash respectively) compared with the mixture containing 0.25 DSF (19.5 cm and 17 cm for 5% and 0% fly ash respectively).

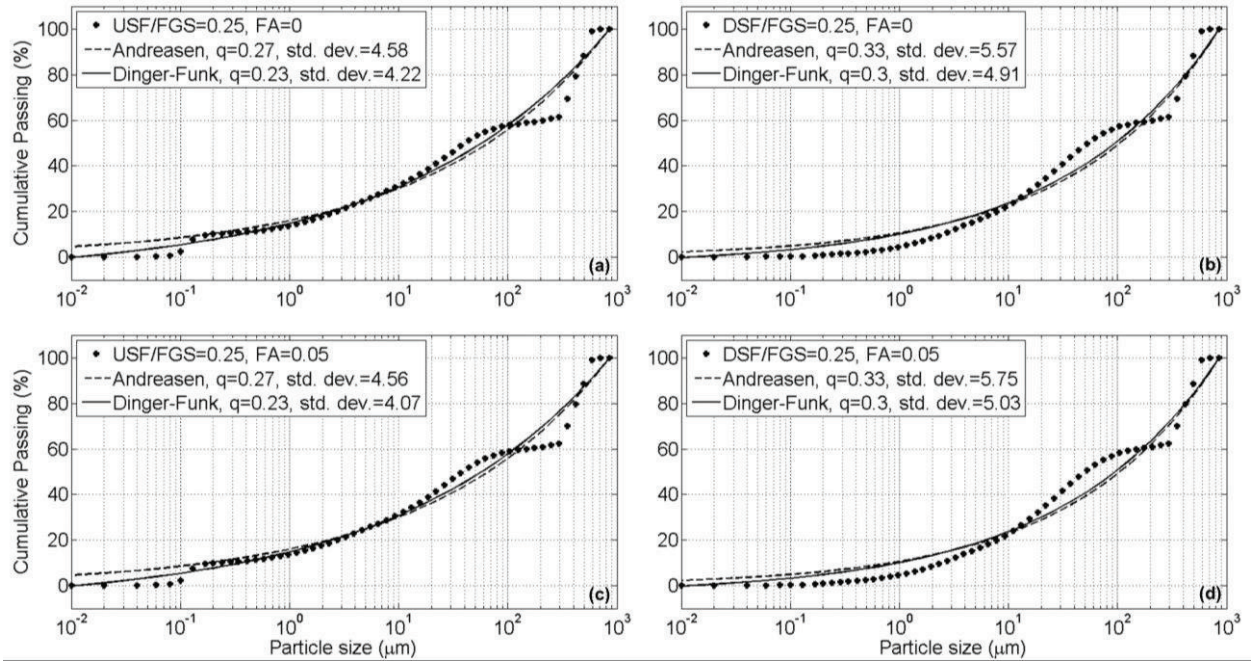

Figure 8 Particle size distribution of mixtures with 0.25 silica fume, 0.25 FGS, and (a) 5% fly ash, (b) 0% fly ash to cement ratio by weight, compared with PSD models

Table 2: Self-consolidating characterization of UHPC

No.	Method	UHPC	EFNARC [12]
1	Slump flow by Abram's cone	77 cm	65-85 cm
2	T_{50cm} slump flow	4 sec	2-5 sec
3	J-ring, height difference	0-2 mm	0-10 mm
4	V-funnel	10 sec	6-12 sec
5	V-funnel increase time at T_{5min}	7 sec	3 sec
6	J-ring, spread difference	0 cm	N/A
7	Visual stability index (ASTM C1611)	0 (no segregation)	N/A
8	Air content	4.8%	N/A
9	Compressive strength	152.72 MPa	N/A

While incorporating a small amount of fly ash (e.g. 5%) did not result in a significant difference in the q value and the standard deviation of the particle size distribution curve, it did improve the flowability of the mixture. The increase in spread value was 3 cm for the mixture with USF, and 2.5 cm for the mixture with DSF. This phenomenon was due to the spherical shape of fly ash particles, which provided a "ball bearing" effect leading to increased flowability.

Table 2 summarizes the self-consolidating characteristics, air content and compressive strength of two self-consolidating UHPC mix designs.

Structural Behavior of S-UHPC Modules

Large-scale structural testing was performed on S-UHPC beams with various cross tie ratios. For the north side of S-UHPC-1 (Figure 9), two flexural cracks appeared during the first loading step. As a result, the north end shear force dropped from 49.64 kN to 40.8 kN. As the step was progressing, existing cracks widened and new cracks developed. Maximum crack width of 5 mm occurred at crack 1 location. The shear force in the north end reached a maximum of 208.7 kN with corresponding net deflection 8.8 mm. For the south side of S-UHPC-1 (Figure 10), an initial flexure crack in the shear span had occurred during the testing of the north end of the specimen, causing a reduction of the initial stiffness of the beam. The second flexure crack occurred at the mid-span region, causing the shear force to drop from 109.2 kN to 102.8 kN, with a corresponding deflection of 3.3 mm. The peak load reached 220.5 kN with a net deflection of 8.6 mm right after the first cross tie yielded. At the peak load, the steel plate did not yield and there was no crushing of the UHPC. The maximum crack width was 2.5 mm. The amount of cross ties in S-UHPC-1 (South) was found to be just sufficient to prevent a premature sudden failure due to debonding between UHPC and steel plate.

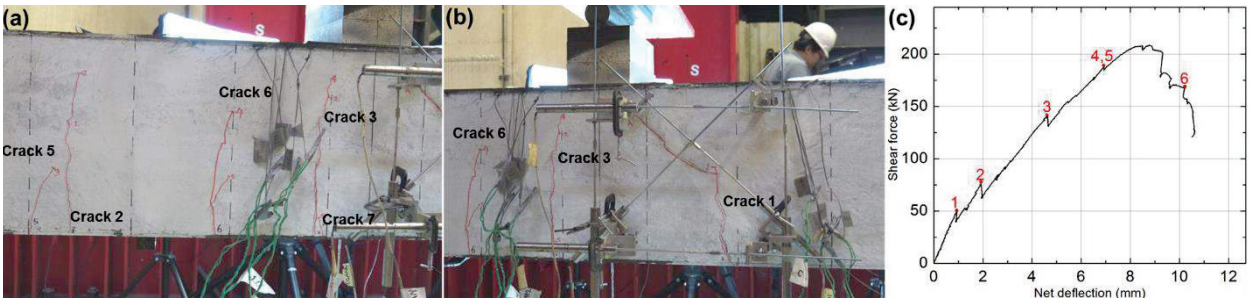

Figure 9 Crack pattern at (a) shear span (b) mid span, (c) shear-force deflection curve for S-UHPC-1 N:
1. Crack (flexural) – shear span, 2. Crack (flexural) – mid span, 3. NBE3 yielded at 143.1 kN,
4. NTE2 yielded at 185.5 kN, 5. NBW3 yielded at 184.7 kN, 6. NME3 yielded at 167.6 kN

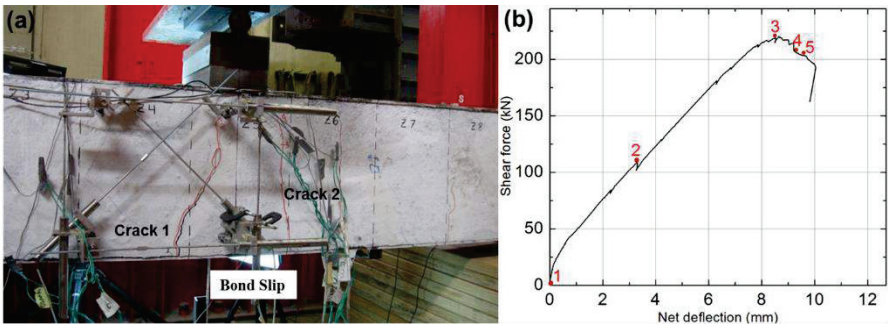

Figure 10 (a) Crack pattern and failure mode, (b) shear-force deflection curve for S-UHPC-1S:
1. Initial flexural crack – shear span, 2. Flexural crack – mid span,
3. SBW2 yielded at 219.7 kN. 4. SBE2 yielded at 207.1 kN, 5. SBE4 yielded at 203.9 kN

For the north end of S-UHPC-2, a flexural crack occurred at the shear span region near the loading point. This crack caused the load to drop from 39.1 kN to 22.4 kN. More flexural cracks occurred as the test progressed. After the cross ties at NBE2 and NBW2 yielded at 179.4 kN and 191.6 kN, the stiffness of the specimen was not decreasing. This may be due to the shear strength contribution of UHPC being higher than the cross ties at this stage. The north steel-plate strain-gauge (NSS) yielded at 309.6 kN, corresponding to the deflection of 10.4 mm. The peak value reached 381.7 kN, which corresponded to a deflection of 41.7 mm. The shear force-deflection curve (Figure 11 (b)) shows that the increased amount of cross ties prevented

premature failure of the beam due to bond slip and increased its total shear carrying capacity. The increased amount of cross ties delayed the debonding between the bottom steel plate and UHPC, thus providing an efficient shear transfer mechanism for the the stresses in the steel plate developed to yield point and beyond.

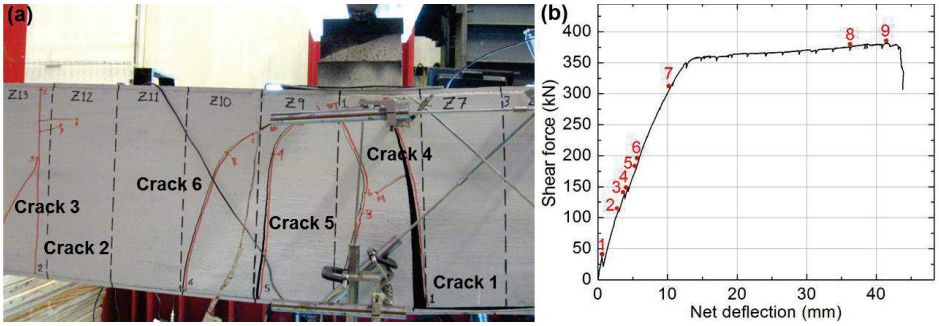

Figure 11 (a) Crack pattern and failure mode, (b) shear-force deflection curve for S-UHPC-2N:
1. Crack (flexural) – shear span, 2. Crack (flexural) – mid span, 3. Visible bond slip,
4. Crack (flexural) – mid span, 5. NBE2 yielded at 179.4 kN, 6. NBW2 yielded at 191.6 kN,
7. NSS yielded at 309.6 kN, 8. NBW3 yielded at 376.3 kN, 9. Peak value at 381.7 kN

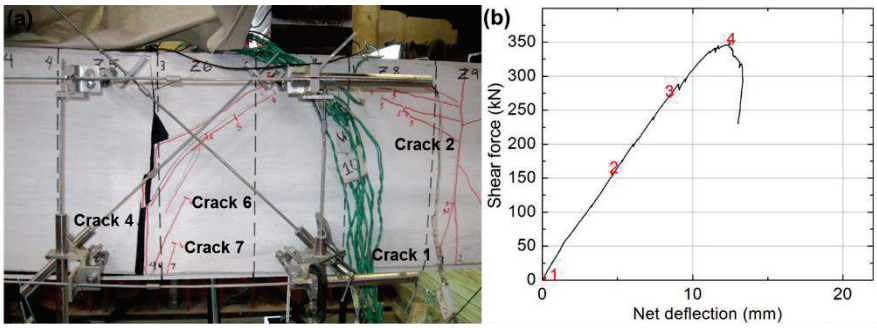

Figure 12 (a) Crack pattern and failure mode, (b) shear-force deflection curve for S-UHPC-2S:
1. Initial cracks and bond slip, 2. SME3 yielded at 154.3 kN, 3. SBE3 yielded at 269.0 kN, 4. Peak at 345.6 kN

Table 3 Experimental matrix and results

Specimen	S (cm)	f_c' (MPa)	$\rho_{t,ACI}$ (%)	$\rho_{t,test}$/ (%)	$\rho_{t,test}$/ $\rho_{t,ACI}$	F_{peak}^{*} (kN)	Ductility δ^{**}	Failure Mode
S-UHPC-1 South	25.4	154.0	0.170	0.184	1.08	220.5	1.003	Ductile
S-UHPC-1 North	20.3	154.0	0.170	0.231	1.35	207.1	1.706	Ductile
S-UHPC-2 South	17.1	153.89	0.170	0.277	1.63	345.6	2.650	Ductile
S-UHPC-2 North	14.6	153.89	0.170	0.323	1.90	381.7	4.010†	Ductile

Note: * peak shear capacity
** shear ductility (deflection at the peak /deflection when cross ties yielded)
† flexural ductility

During the testing of the north end of the specimen, 4 cracks appeared at the south end of the specimen in the shear span and the mid-span region. These cracks reduced the initial stiffness of the specimen. Cross ties at SME3 and SBE3 yielded at 154.3 kN and 269 kN with a corresponding deflection of 4.6 mm and 8.4 mm, respectively. The peak reached 345.6 kN at a net deflection of 12.3 mm. Steel plate did not yield and UHPC was not crushed at peak load. It can be concluded that the shear reinforcement ratio was sufficient to prevent premature bond failure and increased the shear carrying capacity of the SC beam. However, the

cross ties were not sufficient to maintain the bond until yielding of the bottom steel plate. Table 3 shows the experimental matrix and the summary of the results for the two S-UHPC beams.

Based on the structural testing results, the minimum cross tie area ($\rho_{t,min}$) of 10% more than the minimum required by ACI 349 code ($\rho_{t,ACI}$) is recommended for S-UHPC beams. Thus, $\rho_{t,min}$ is equal to 1.10 of $\rho_{t,ACI}$ for S-UHPC beams.

CONCLUSION

A new type of self-consolidating UHPC was developed for nuclear power plant applications. The material can be robustly processed at large scale with commercially available ingredients and equipment, and meet self-consolidating and compressive strength requirements. Particle size distribution for optimum packing density, the physical and chemical parameters of ingredients, and the resulting microstructure after hydration are considered essential for the design of self-consolidating UHPC. This study also led to the establishment of the rational minimum cross tie ratio for S-UHPC beams. Currently, SC structures are designed using ACI 349, adopting the considerations of ACI 318 that was developed for reinforced concrete structures. However, this study suggested 1.10 $\rho_{t,ACI}$ for S-UHPC beams to ensure ductile shear behavior. The results from this study will pave the way for the application of a new generation of self-consolidating UHPC material and S-UHPC modules for SMRs or nuclear power plants.

ACKNOWLEDGEMENTS

The research described in this paper is financially supported by U.S. Department of Energy NEUP program (Project No. CFP-13-5282). The opinions expressed in this study are those of the authors and do not necessarily reflect the views of the sponsors.

REFERENCES

Brouwers, H. J. H. and Radix, H. J. (2005). "Self-Compacting Concrete: the Role of the Particle Size Distribution," *Paper presented at the First International Symposium on Design, Performance and Use of Self-Consolidating Concrete*, Changsha, Hunan, China.

Elkem. (2014). *Elkem Materials Mixture Analyzer*.

Ferguson, P. M. and Clark, A. P. (1951). "Diagonal Tension in Reinforced Concrete," *ACI Journal*, 48(2), 156-151 to 156-153.

Funk, J. E. and Dinger, D. (1928). *Perdictive Process Control of Crowded Particulate Suspensions: Applied to Ceramic Manufacturing*. Norwell: Kluwer Academic Publishers.

Kani, G. (1964). "The Riddle of Shear Failure and Its Solution," *ACI Journal*, 61(4), 441-467.

Larrard, F. D. (1992). *Ultrafine Particles for Making Very High Performance Concrete High Performance Concrete: from Material to Structure* (pp. 34-47). London: E & FN Spon.

Qin, F., Tan, S., Yan, J., Li, M., Mo, Y. L., and Fan, F. (2015). *Minimum Shear Reinforcement Ratio of Steel Plate Concrete Beams.*

Subedi, N. (2003). "Double skin steel/concrete composite beam elements: experimental testing," *Structural Engineer*, 81(21), 30-35.

Varma, A. H., Sener, K. C., Zhang, K., Coogler, K., and Malushte, S. R. (2011). "Out-of-plane Shear Behavior of SC Composite Structures," *International Association for Structural Mechanics in Reactor Technology 21*.

Xie, M., Foundoukos, N., and Chapman, J. (2007). "Static tests on steel–concrete–steel sandwich beams," *Journal of Constructional Steel Research*, 63(6), 735-750.

Yu, R., Spiesz, P., and Brouwers, H. (2014). "Mix design and properties assessment of Ultra-High Performance Fibre Reinforced Concrete (UHPFRC)," *Cement and concrete research*, 56, 29-39.